Molecularly Tailored Artesunate Nanomedicine with Well-balanced Nanoassembly and Anticancer Performance

Haonan Wu[1#], Xuan Zhang[1#], Xiaomei Shu[1], Hongyuan Zhang[1], Wenhu Zhou[2,3], Shenwu Zhang[1,4*], Cong Luo[1,4*]

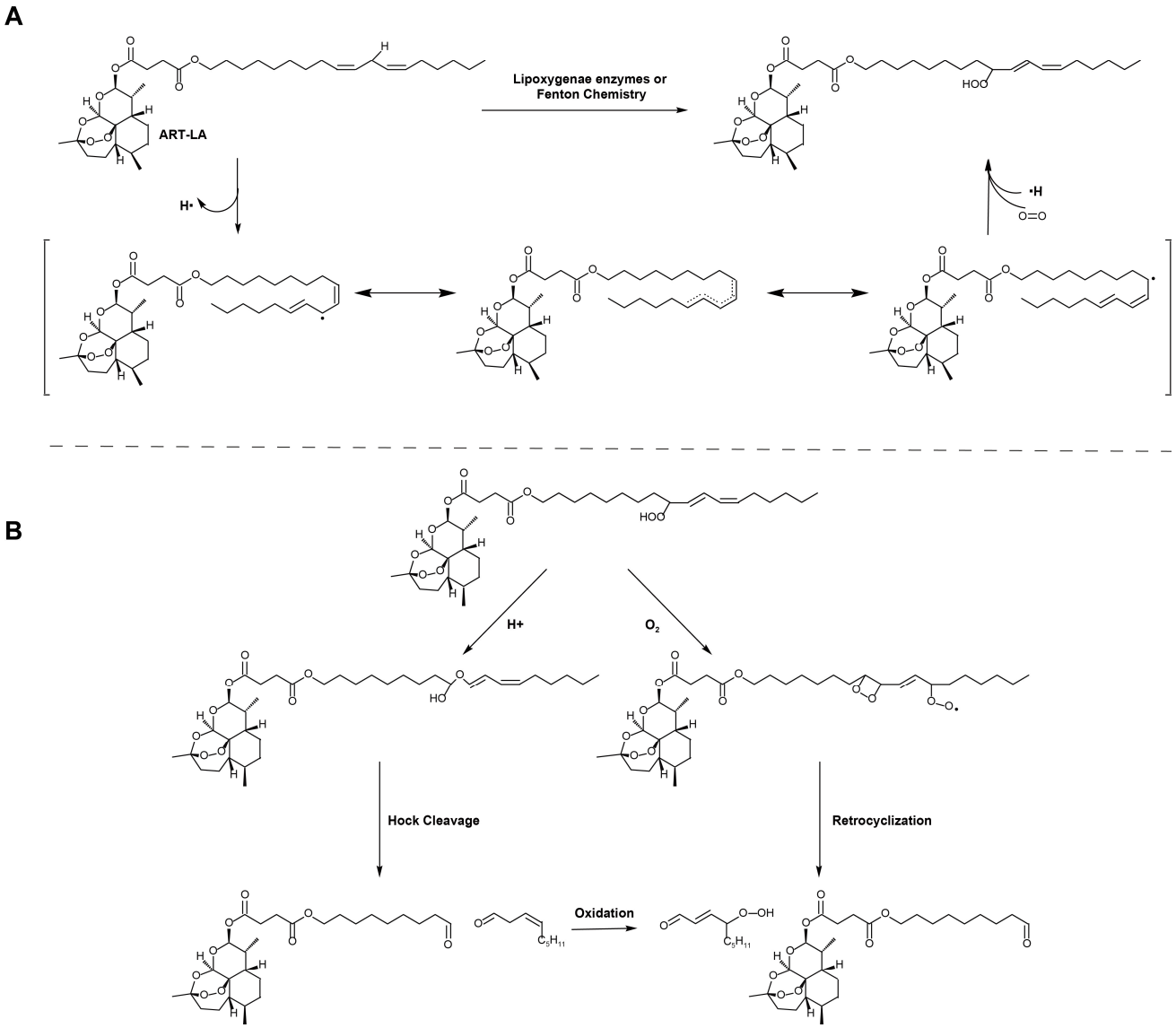


Figure S1. Schematic diagram of the oxidative cleavage mechanism of ART-LA. (A) The process of lipid peroxidation in ART-LA. (B) Degradation of lipid peroxides.

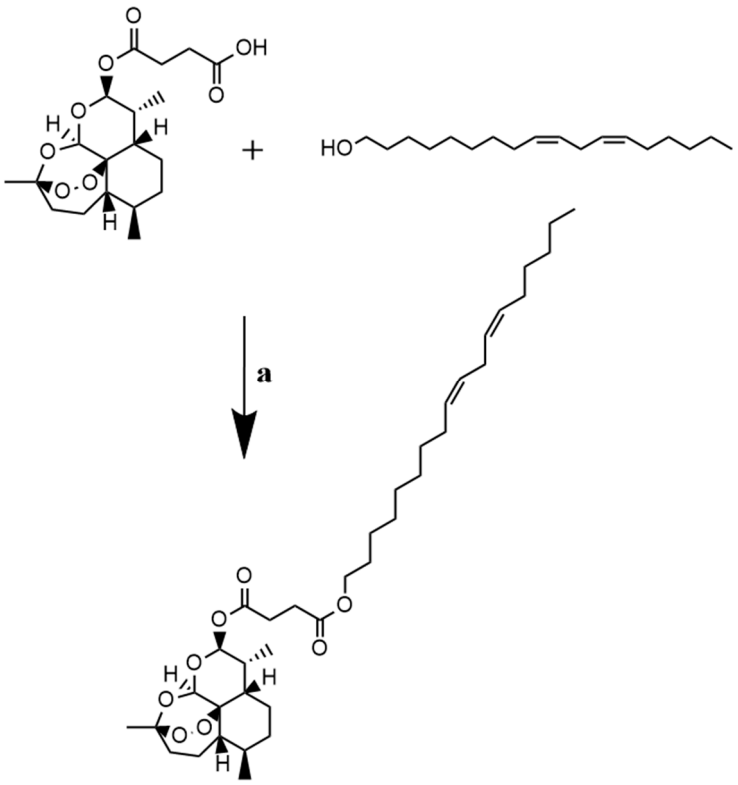


Figure S2. The synthetic route of ART-LA, (a) DMAP, EDCI, 25℃.

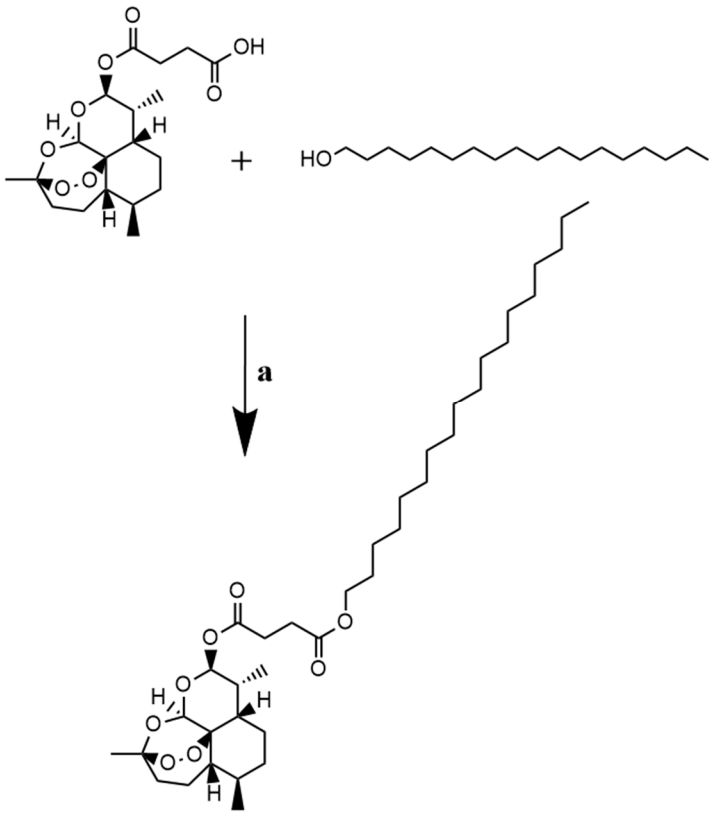
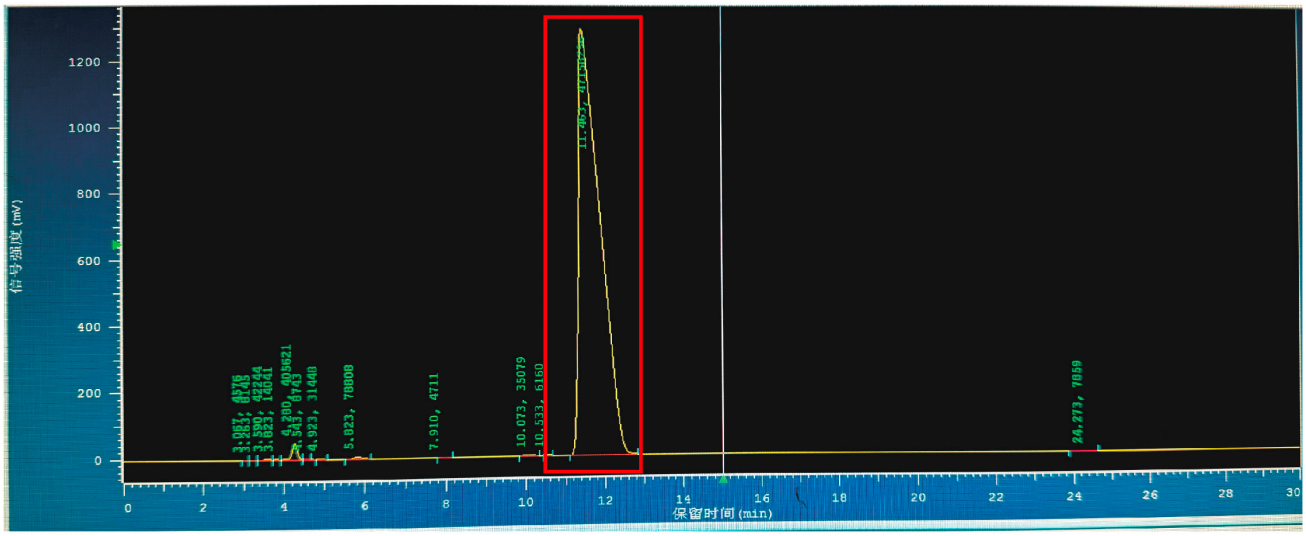


Figure S3. The synthetic route of ART-SA, (a) DMAP, EDCI, 25℃.

A

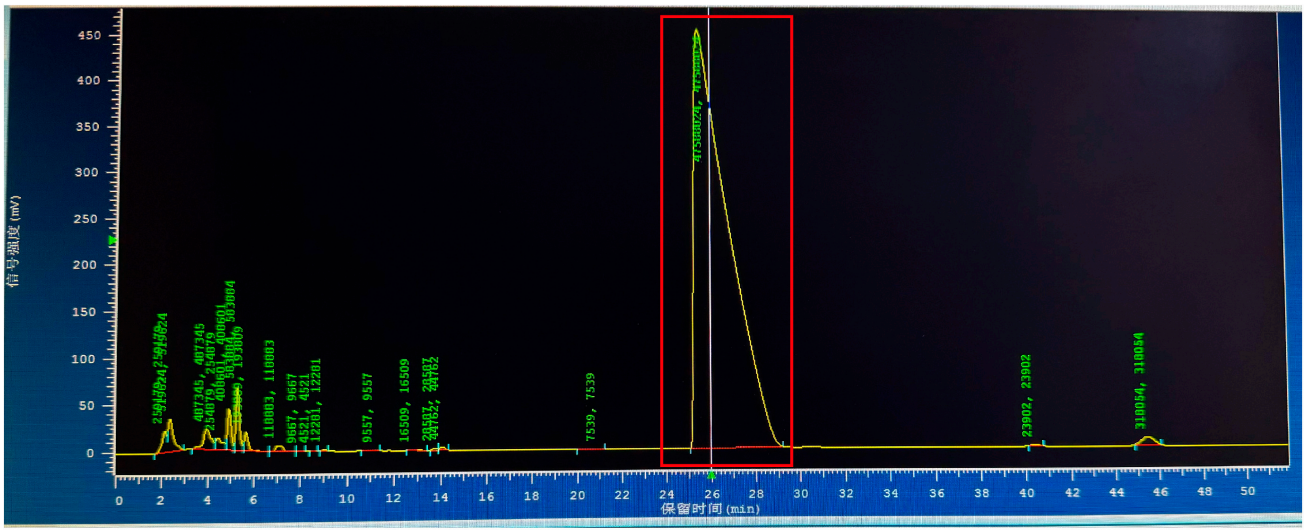


B

No.	RT	AREA	CONC1	BC	
1	3.067	4576	0.010	BV	
2	3.263	8145	0.017	VV	
3	3.590	42244	0.088	VV	
4	3.823	14041	0.029	VV	
5	4.280	405621	0.848	VV	
6	4.543	8743	0.018	TBB	
7	4.923	31448	0.066	VB	
8	5.823	78808	0.165	BB	
9	7.910	4711	0.010	BB	
10	10.073	35079	0.073	BB	
11	10.533	6160	0.013	BB	
12	11.463	47158256	98.646	BB	**The purity of ART-LA: 98.6%**
13	24.273	7859	0.016	BB	
		47805691	100.000		

Figure S4. (A) The high-performance liquid chromatogram of ART-LA. (B) The HPLC purity percentages of ART-LA.

A



B

No.	RT	AREA	CONC1	BC	
1	2.160	259179	0.511	BV	
2	2.373	519624	1.024	VB	
3	3.973	484256	0.955	BV	
4	4.467	251143	0.495	VV	
5	4.933	404762	0.798	VV	
6	5.293	578912	1.141	VV	
7	5.673	176404	0.348	VB	
8	7.033	118883	0.234	BB	
9	7.987	5810	0.011	BB	
10	9.013	12281	0.024	BB	
11	11.213	9557	0.019	BB	
12	12.787	16509	0.033	BB	
13	14.080	68065	0.134	BB	
14	25.427	47523374	93.679	BB	**The purity of ART-SA: 93.7%**
15	40.373	23902	0.047	BB	
16	45.427	277179	0.546	BB	
		50729840	100.000		

Figure S5. (A) The high-performance liquid chromatogram of ART-SA. (B) The HPLC purity percentages of ART-SA.

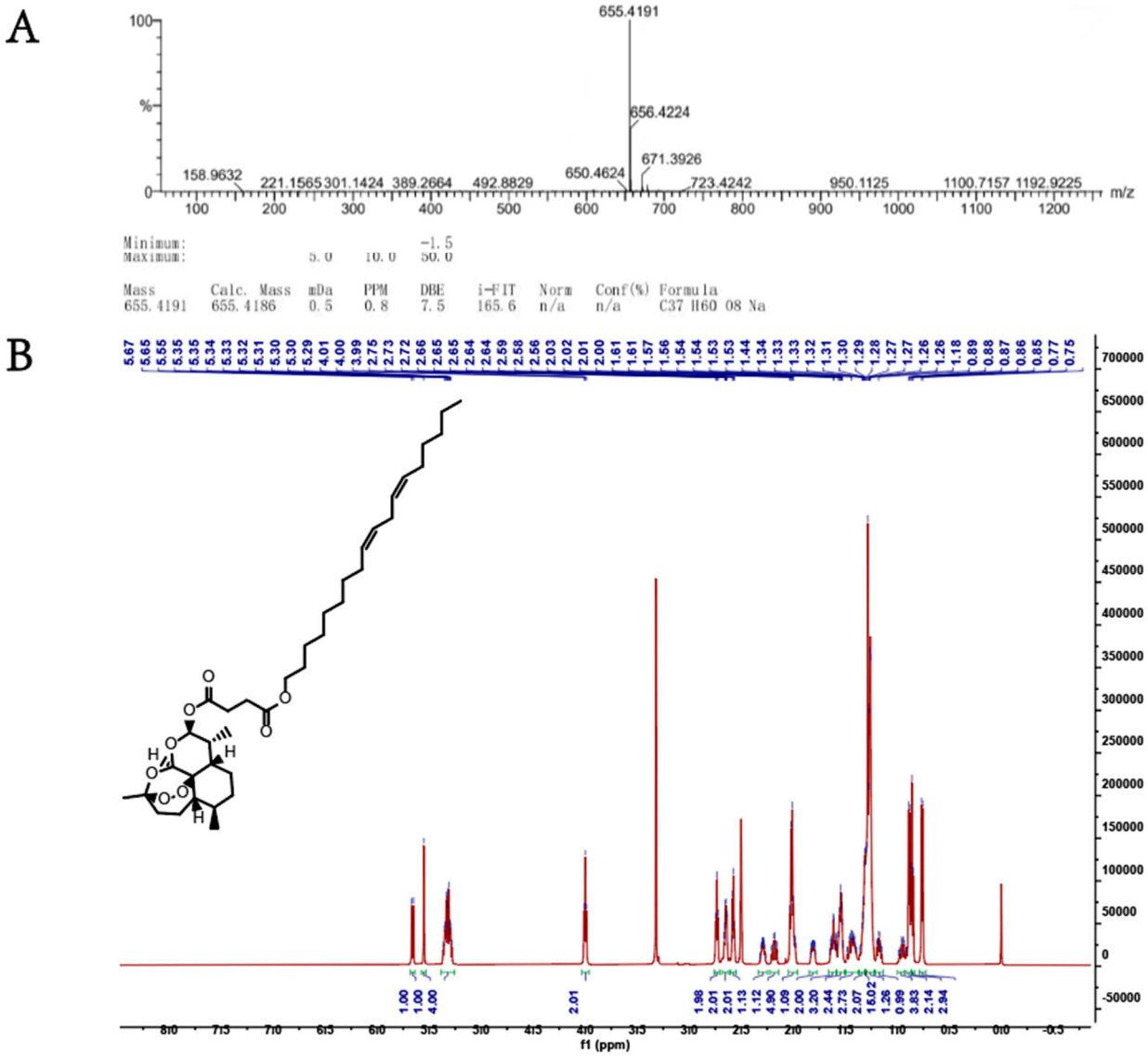


Figure S6. (A) MS of ART-LA. $[M + Na]^-$ = 655.42. (B) ^{1}H NMR of ART-LA. ^{1}H NMR (600 MHz, DMSO-d6) δ 5.66 (d, J = 9.7 Hz, 1H), 5.55 (s, 1H), 5.32 (tdd, J = 17.9, 11.1, 7.0 Hz, 4H), 4.00 (t, J = 6.6 Hz, 2H), 2.73 (t, J = 6.8 Hz, 2H), 2.65 (td, J = 6.0, 5.6, 3.4 Hz, 2H), 2.58 (t, J = 6.2 Hz, 2H), 2.34 – 2.25 (m, 1H), 2.18 (td, J = 14.0, 3.9 Hz, 1H), 2.02 (q, J = 6.8 Hz, 5H), 1.81 (ddt, J = 13.7, 6.9, 3.5 Hz, 1H), 1.62 (tt, J = 13.9, 3.3 Hz, 2H), 1.59 – 1.51 (m, 3H), 1.50 – 1.37 (m, 2H), 1.33 (d, J = 15.4 Hz, 3H), 1.30 (s, 2H), 1.30 – 1.22 (m, 15H), 1.17 (td, J = 11.4, 6.6 Hz, 1H), 1.00 – 0.93 (m, 1H), 0.92 – 0.86 (m, 4H), 0.85 (d, J = 7.1 Hz, 2H), 0.76 (d, J = 7.1 Hz, 3H).

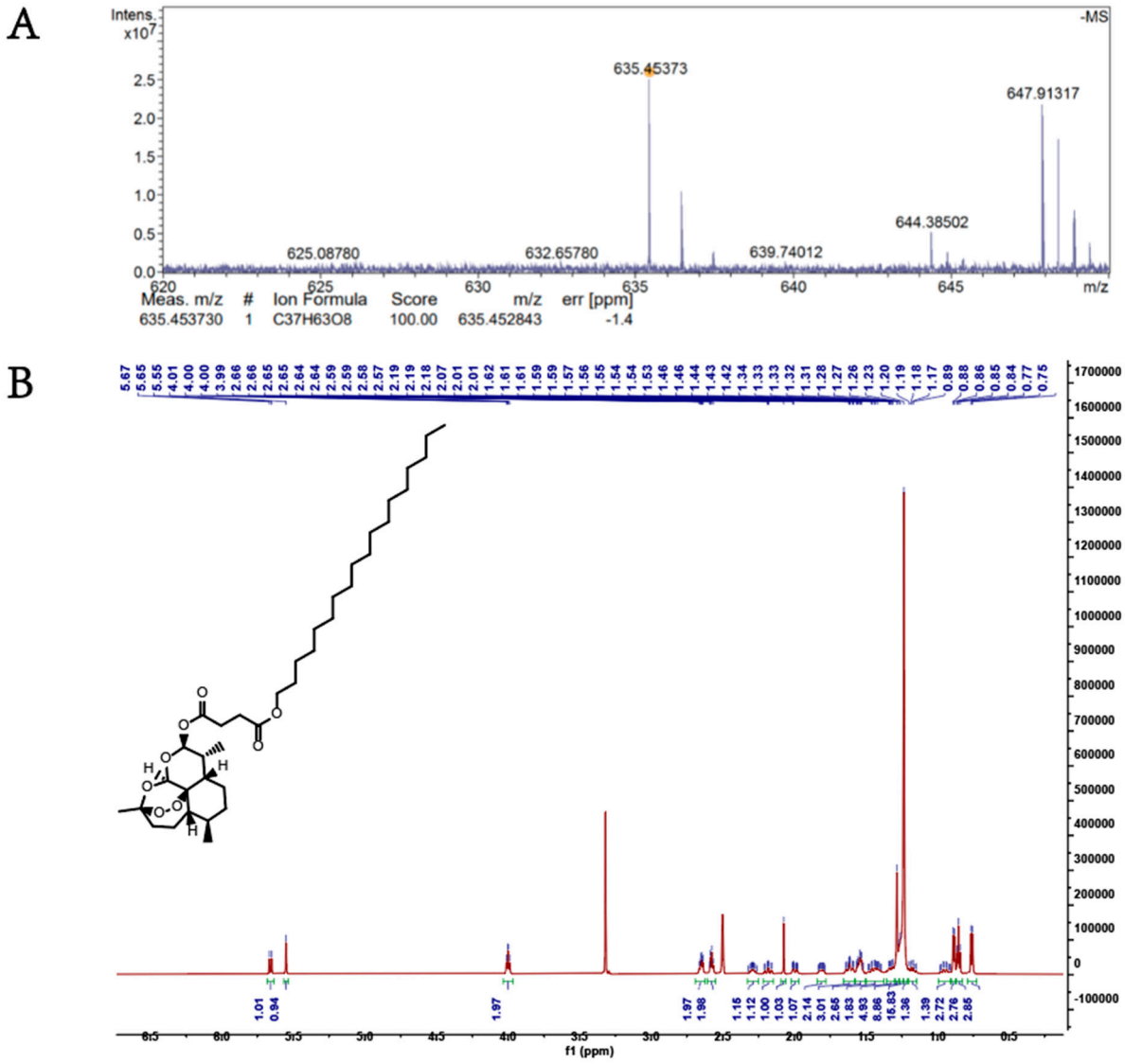


Figure S7. (A) MS of ART-SA. $[M - H]^-$ = 635.45. (B) ^{1}H NMR of ART-SA. ^{1}H NMR (600 MHz, DMSO-d6) δ 5.66 (d, J = 9.7 Hz, 1H), 5.55 (s, 1H), 4.03 – 3.97 (m, 2H), 2.65 (td, J = 6.0, 5.4, 3.7 Hz, 2H), 2.58 (t, J = 6.2 Hz, 2H), 2.33 – 2.25 (m, 1H), 2.22 – 2.15 (m, 1H), 2.07 (s, 1H), 2.00 (ddd, J = 14.5, 5.0, 3.0 Hz, 1H), 1.81 (ddt, J = 13.6, 6.8, 3.5 Hz, 1H), 1.62 (tq, J = 16.9, 3.3 Hz, 2H), 1.54 (tt, J = 10.9, 5.1 Hz, 3H), 1.50 – 1.37 (m, 3H), 1.35 – 1.30 (m, 2H), 1.28 (s, 5H), 1.26 (s, 9H), 1.23 (s, 16H), 1.17 (td, J = 11.4, 6.7 Hz, 1H), 0.95 (qd, J = 13.2, 12.6, 3.9 Hz, 1H), 0.89 (d, J = 6.4 Hz, 3H), 0.85 (t, J = 6.9 Hz, 3H), 0.76 (d, J = 7.1 Hz, 3H).

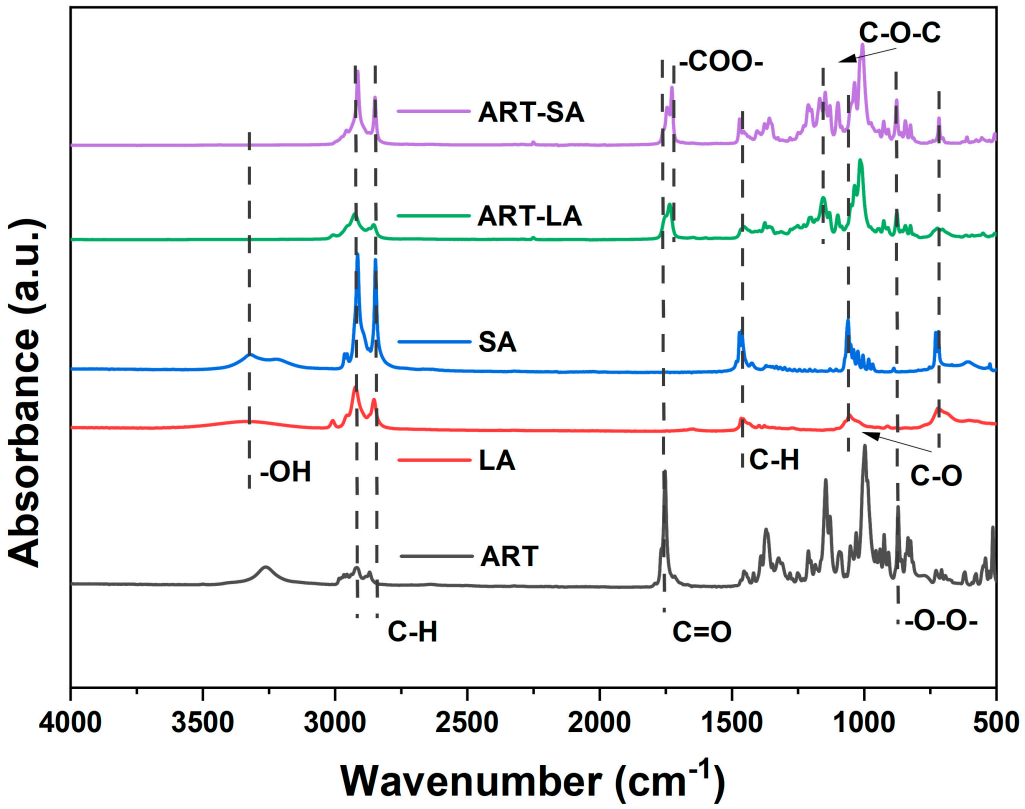


Figure S8. FTIR of ART, LA, SA, ART-LA, and ART-SA.

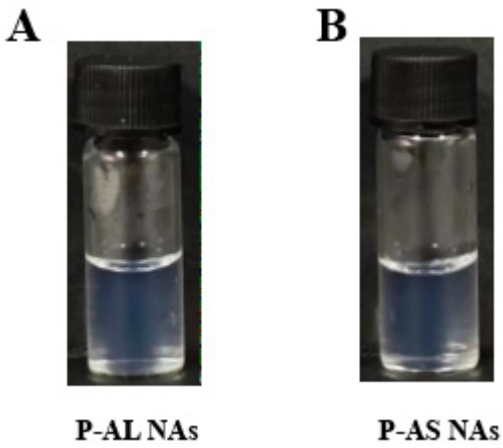


Figure S9. Appearance of the preparation，(A) P-AL NAs, and (B) P-AS NAs.

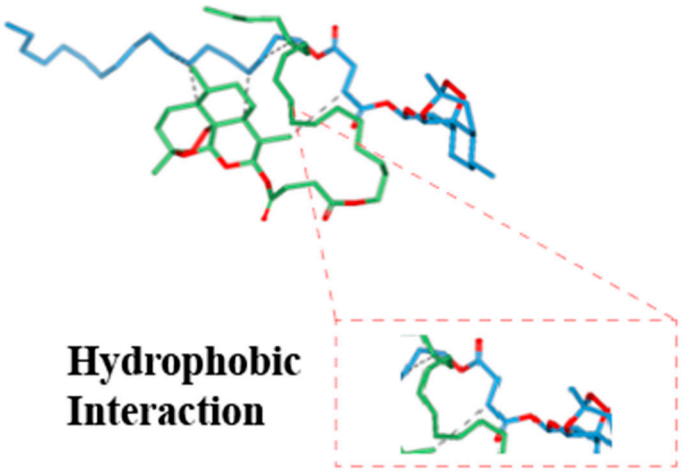


Figure S10. Molecular docking simulation of P-AS NAs.

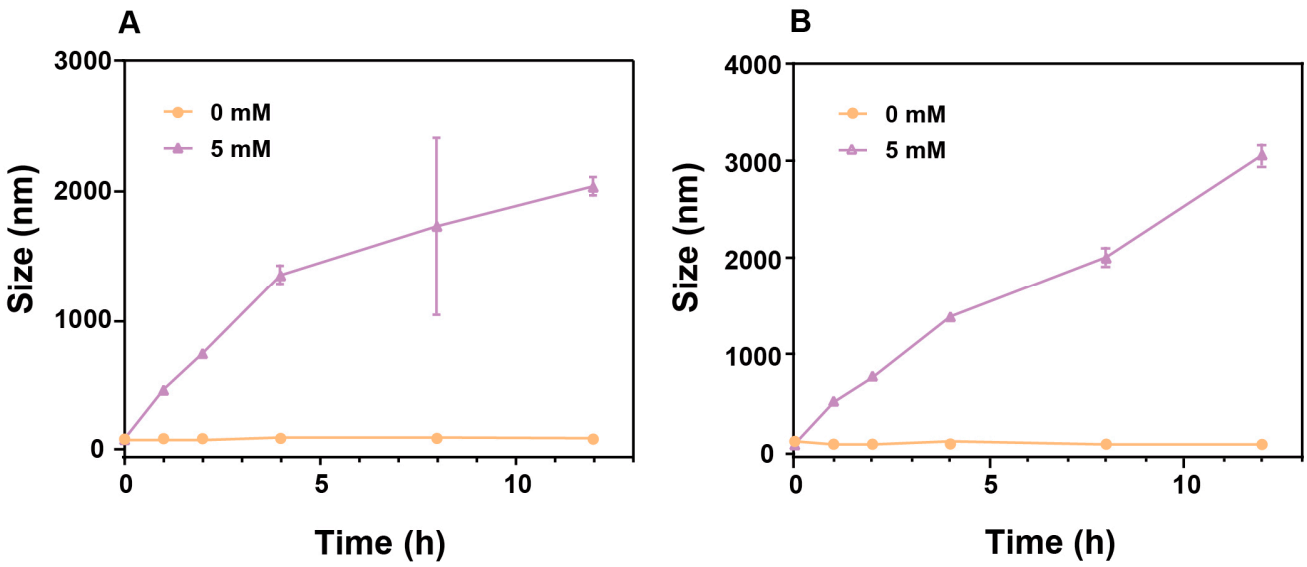


Figure S11. (A) The particle size of P-AL NAs varies under different DTT concentrations. (B) The particle size of P-AS NAs varies under different DTT concentrations.

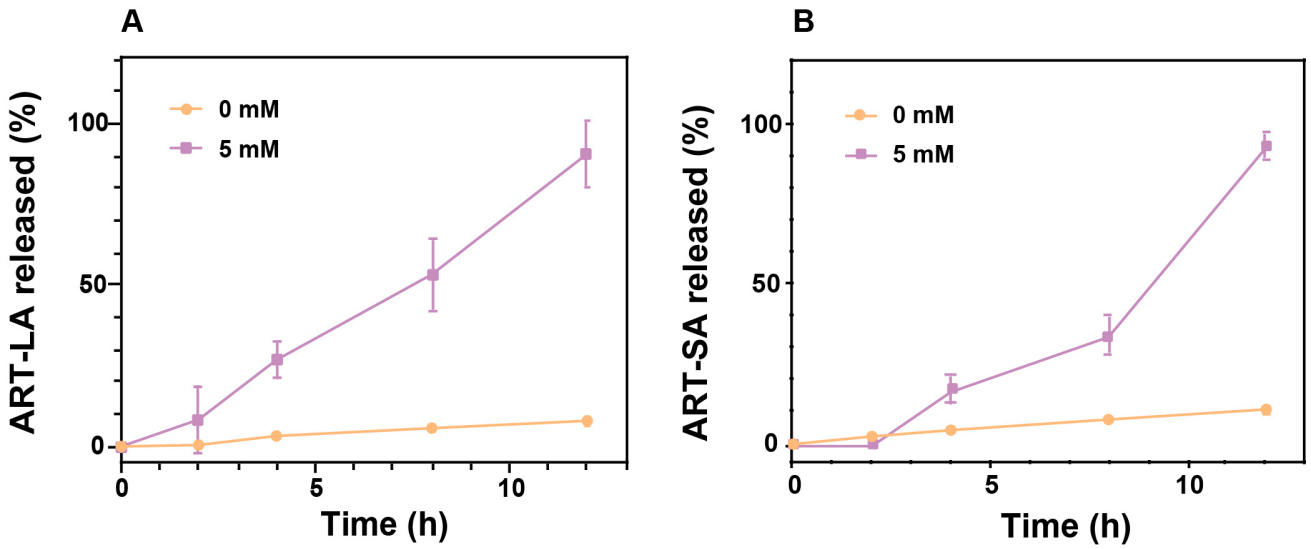


Figure S12. (A) The release curves of ART-LA in P-AL NAs under different DTT concentrations. (B) The release curves of ART-SA in P-AS NAs under different DTT concentrations.

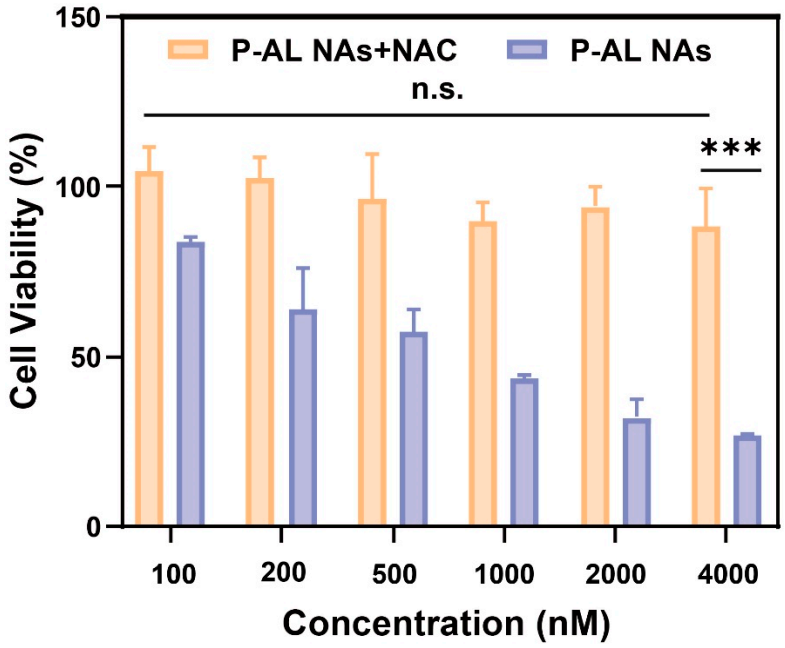


Figure S13. The effect on the antitumor activity of P-AL NAs (equal amounts of ART from 0 to 4000 nM) under the conditions with or without NAC (5 mM) ($n = 3$). Data are presented as the mean ± SD. Intergroup significant differences were evaluated using Student's t-test. n.s. represents $p > 0.05$, *** represents $p < 0.001$.

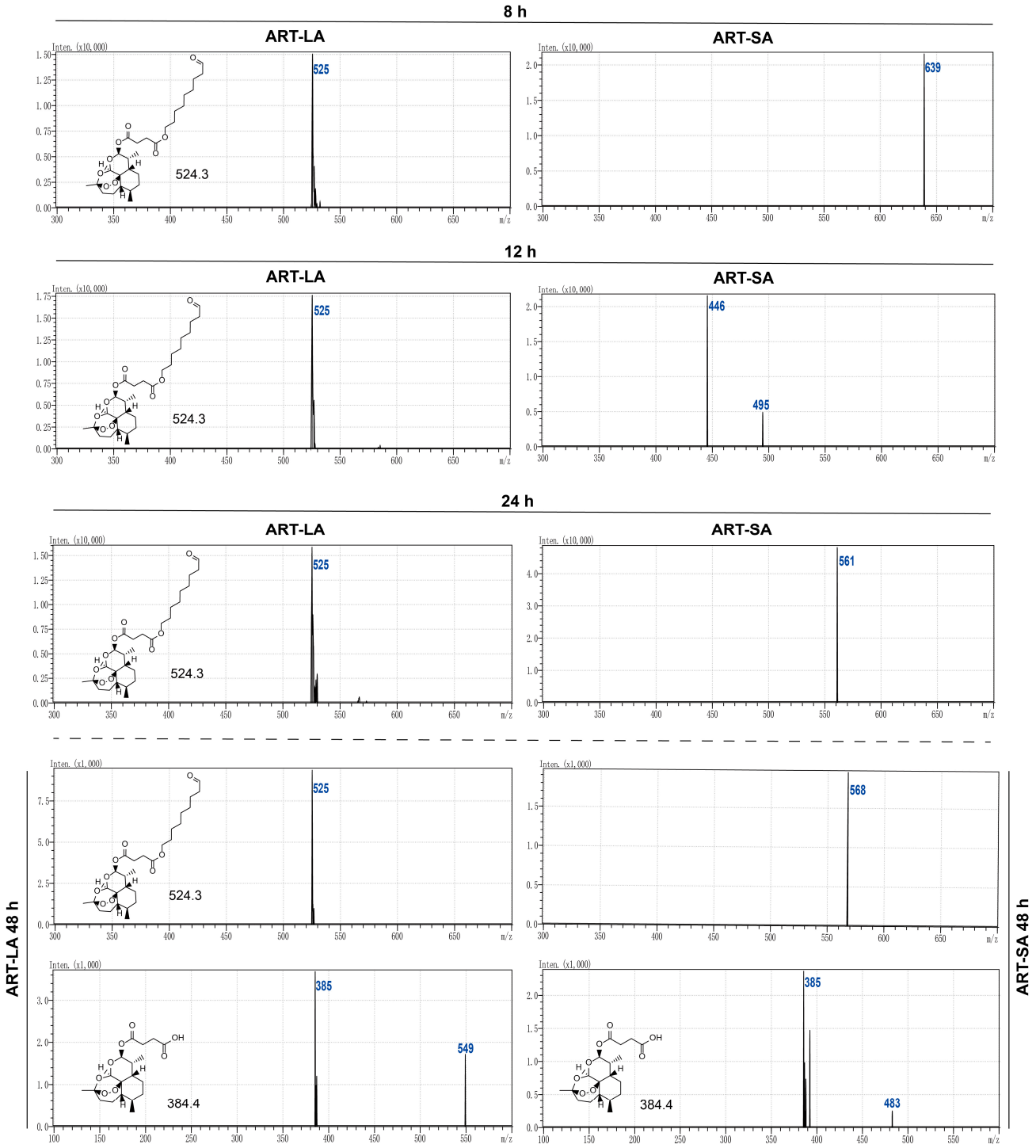


Figure S14. Intermediates of ART-LA and ART-SA produced after lipid peroxidation at different time.

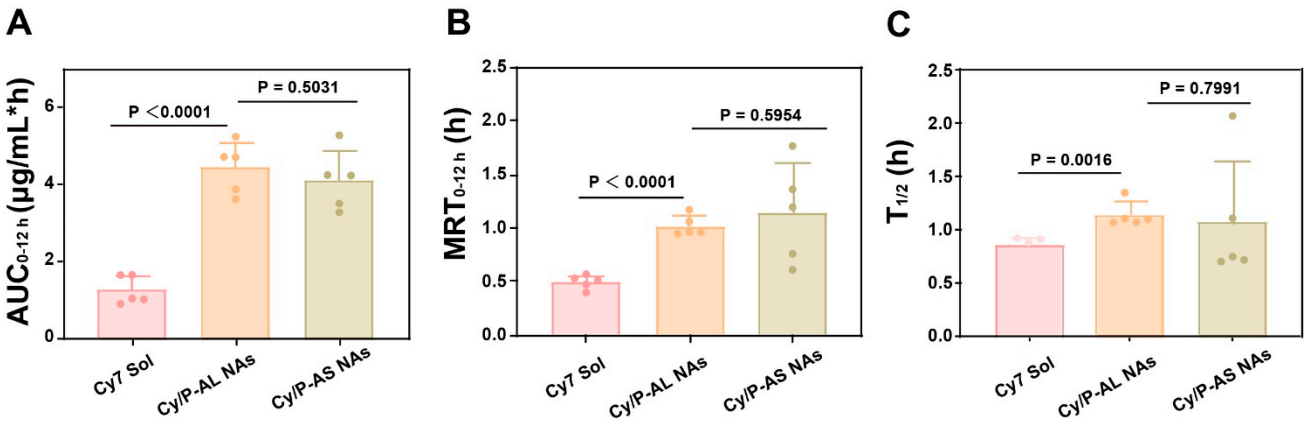


Figure S15. Detailed mathematical statistical chart of pharmacokinetic parameters. (A) $AUC_{0\text{-}12\ h}$; (B) $MRT_{0\text{-}12\ h}$; (C) $T_{1/2}$.

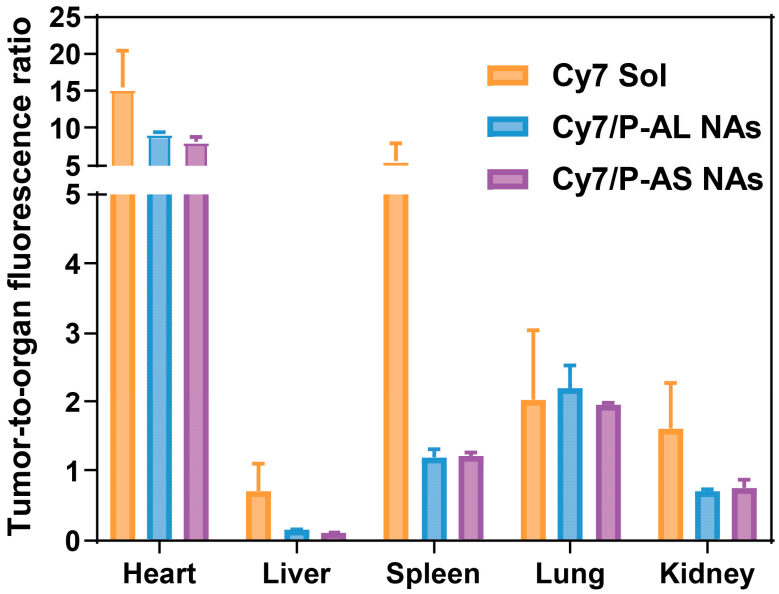


Figure S16. The quantitative tumor-to-organ fluorescence ratio of Cy7 Sol, Cy7/P-AL NAs, and Cy7/P-AS NAs at 6 h after administration (n = 3).

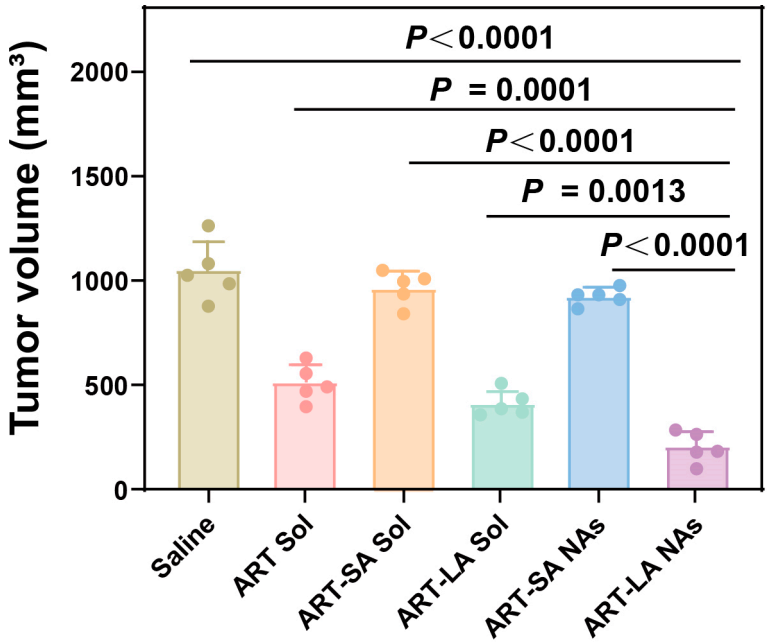


Figure S17. Detailed mathematical plots of tumor volumes treated by different treatment groups at day 9.

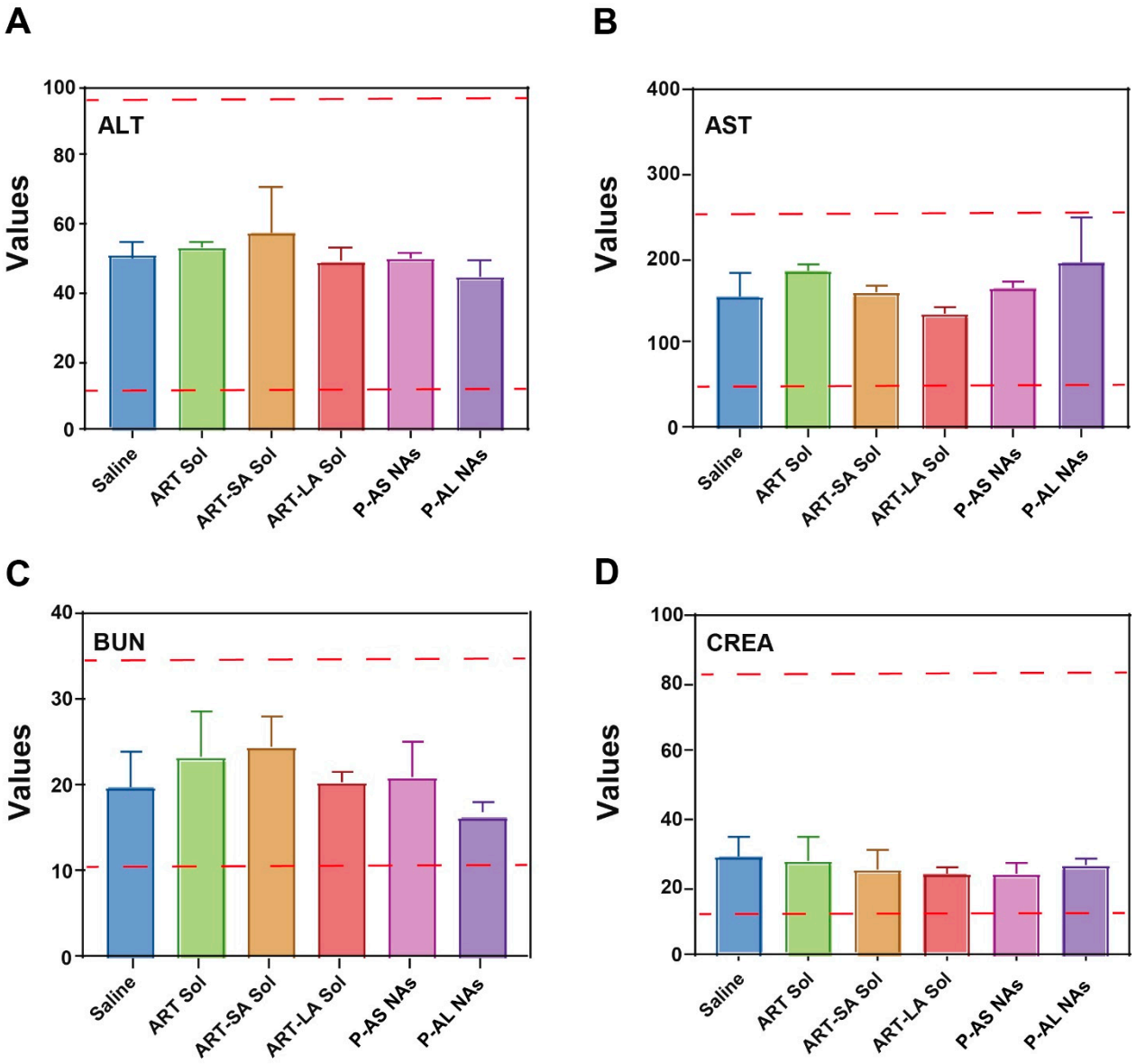


Figure S18. Serum biochemical analysis for ALT (A), AST (B), BUN (C), CREA (D) indicators (n = 3).

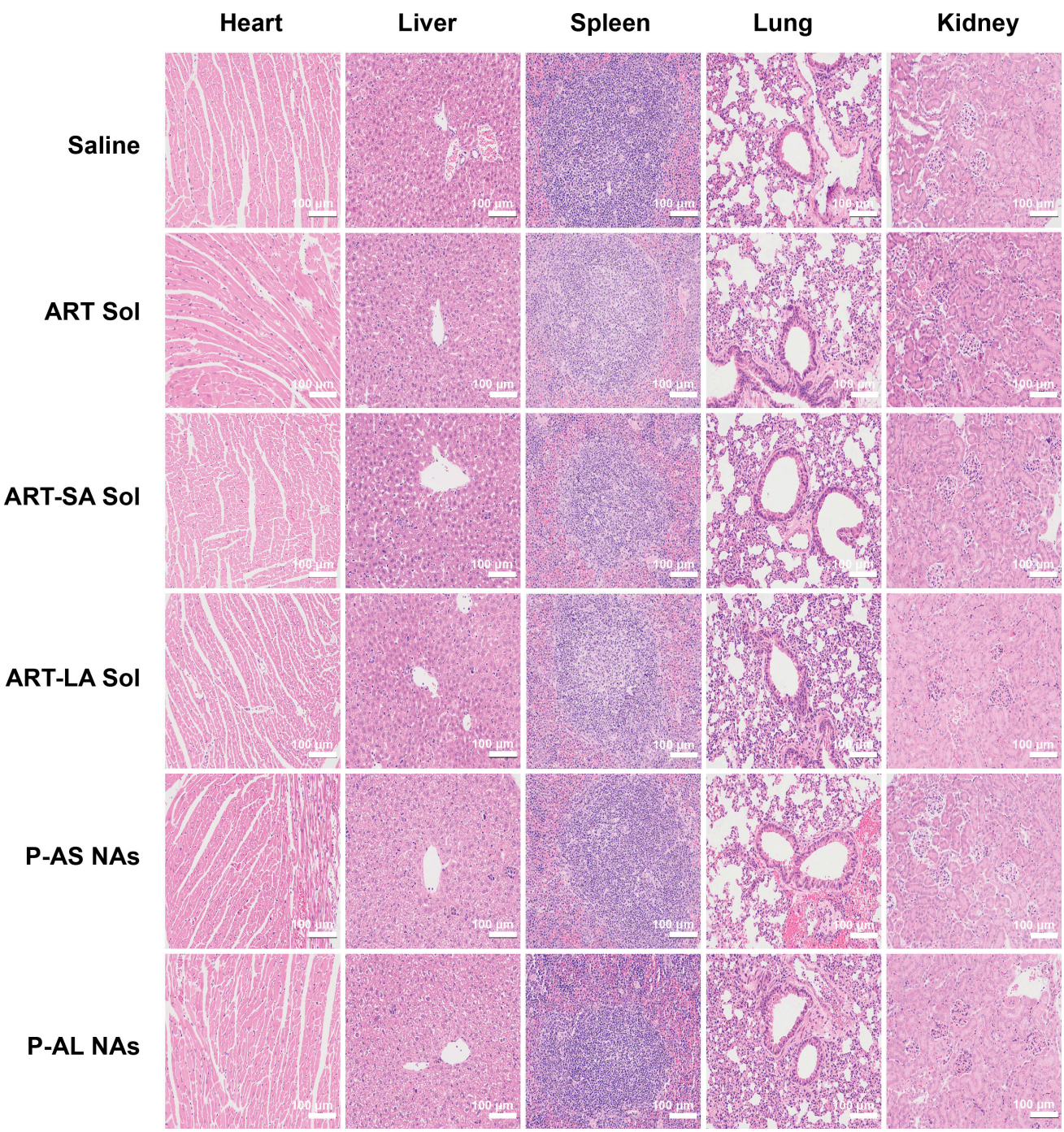


Figure S19. The H&E staining images of heart, liver, spleen, lung and kidney after different treatments (scale bar = 100 μm).

Table S1. Characterization of P-AL NAs and P-AS NAs.

Formulations	[a)]Size (nm)	[b)]PDI	[c)]Zeta potential (mV)
P-AL NAs	78.78 ± 1.35	0.08 ± 0.06	-23.8 ± 0.4
P-AS NAs	80.60 ± 0.66	0.11 ± 0.07	-24.7 ± 0.7

[a-c)] Mean size, polydispersity index and zeta potential of NAs were determined by DLS.

Table S2. Pharmacokinetic parameters of SD rats after various treatments (n = 5).

Formulations	$AUC_{0\text{-}12\ h}$ (μg/mL*h)	$t_{1/2}$ (h)	$MRT_{0\text{-}12h}$ (h)
Cy7 Sol	1.269 ± 0.368	0.865 ± 0.063	0.496 ± 0.065
Cy7/P-AL NAs	4.452 ± 0.668	1.145 ± 0.118	1.019 ± 0.095
Cy7/P-AS NAs	4.128 ± 0.785	1.074 ± 0.587	1.136 ± 0.465